



A Three-Step Hill Neuromusculoskeletal Model Parameter Identification Method Based on Exoskeleton Robot

Pengchen Lian^{1,2,3} · Yue Ma^{1,2} · Liangsheng Zheng^{1,2,3} · Yang Xiao^{1,2,4} · Xinyu Wu^{1,2}

Received: 1 October 2021 / Accepted: 27 January 2022 / Published online: 26 February 2022
© The Author(s), under exclusive licence to Springer Nature B.V. 2022

Abstract

Different from functional alternative equipments such as prostheses, the highly human-machine collaboration performance are required in exoskeleton robots. At present, the commonly used physical human-machine interface can only obtain motion after the movement occurs. Therefore, it is difficult to predict the non-rhythmic movement. The inherent intent detection hysteresis exist in the physical human-machine interface. The cognition based human-machine interface directly detect the neural electrical signals of the human body, and has the characteristics of advanced motion detection. However, the existing methods based on the Hill muscle mechanics model mostly set muscle parameters based on experience. It is difficult to accurately predict joint torque of different subjects because of the parameter difference of the muscle model. Therefore, in this paper, we proposes a three-step muscle parameters identification paradigm for Hill muscle model based on exoskeleton robots. Then, the Adam optimizer with variable learning rate is employed to identify the muscle parameters. Eight healthy subjects are participated in the experiment. The results show that the proposed Adam optimizer with variable learning rate can make the parameters stably convergence. The estimated torque of the identified Hill muscle model have lower error than that of the neural network-based method. The performance of the proposed method is competitive with that of the State-of-art method.

Keywords Exoskeleton robot · Hill muscle model · Human-machine-interface

1 Introduction

The lower limb exoskeleton robot is an effective motion assist equipment that can improve the wearer's mobility with heavy load or Impairment of motor function. The researches of lower extremity exoskeleton robots has been developed rapidly in recent years and has been widely studied in the fields of medical rehabilitation [1], load transportation [2] and walking assist [3–5]. Different from functional alternative equipments such as prostheses, the highly human-machine collaboration performance are required in exoskeleton robots. The basis of human-machine collaboration is the human-machine interface. Therefore, human-machine interface has become one of the

key technologies in controlling of lower-limb exoskeleton robots.

According to the detection targets, there are mainly two types of human-machine interfaces for lower extremity exoskeleton robots currently [6]. The one is the physical based human-machine interfaces which is to constructed through sensors that detect motion, such as IMU [7] and interaction force [8, 9] based physical human-machine interfaces. This type of human-machine interfaces can only collect the information after the movement occurs. This kind of human-machine interfaces is difficult to predict the non-rhythmic movement especially. Therefore, this type of human-machine interface has an inherent hysteresis of intent detection. The second one is the cognition based human-machine interface which is to constructed by detecting the human neuroelectric signal, for example, the electroencephalograph (EEG) or surface electromyography (sEMG) based human-machine interface [10]. The advantage of this kind of human-machine interface is the advanced detection of motion. However, the EEG signal has a low signal-to-noise ratio (SNR) and

✉ Yue Ma
yue.ma@siat.ac.cn

Extended author information available on the last page of the article.

complex patterns, which makes it difficult to use for real-time control. Therefore, the researches on sEMG signals based human-machine interfaces have been conducted in controlling of exoskeleton robots.

There are three main ways to apply sEMG signals to exoskeleton robots: The first one is to evaluate the effect of the exoskeleton robot's gait or assist mode by the sEMG signals of the main muscles of the lower limbs [11–13], and then provide the optimization direction of power assist control offline. The second way is to switch and control the fixed motion modes by sEMG based pattern recognition. D. Llorente-Vidrio et al. [14] proposed presents an event driven automatic controller which employs the sEMG as the trajectory selector. L. Zhang et al. [15] proposed the sEMG and multilayer perceptron neural network based walking pattern selector to control the lower limb exoskeleton robot. H.-J. Liu et al. [16] proposed the sEMG and adaptive neuro-fuzzy inference system (ANFIS) based selector to find proper parameters that are better suited for different subjects. Although the EMG signal can accurately identify a variety of patterns, these patterns are relatively fixed and discrete, and cannot be applied to continuous motion control. The third category is the sEMG based torque estimation control method. According to different modeling methods, this kind of method can be further divided into two sub-categories: machine learning-based methods and biomechanical model-based methods. Machine learning based methods usually employ linear regression models or neural networks to estimate joint torque through sEMG signals, and then implement the control of exoskeleton robots based on the estimated torque. Z. Li et al. [17] proposed the nonlinear normalization method to estimate joint torque and then cascade the Kalman filter to smooth the torque curve. The estimated torque are tracked by a PD controller afterward. K. Kiguchi et al. [18] proposed a linear regression model to estimate the multi-joint torque by sEMG signal. Similarly, K. Gui et al. [19] employed the linear regression model to estimate torque in the exoskeleton robot controller as well. To solve the disadvantages of insufficient torque accuracy of linear regression model, G. Yin et al. [20] proposed the sEMG and bayesian fusion algorithm based method to regress the gait cadence. Besides, [21–25] proposed a series of nonlinear regression methods based on neural networks. The model based on machine learning is simple and convenient, but lacks interpretability, and it is difficult to adjust the delay, gain and other characteristics of the model. The biomechanical model-based methods usually employ Hill-based muscle model to estimate joint torque. D. Ao et al. [26, 27] employed the Hill model to estimate the torque of ankle joint to control the exoskeleton robot. H. Liu et al. [28] proposed a sEMG signals based and combining the regression method with the classification

method human robot cooperative control framework to control the pneumatic upper limb exoskeleton in accordance with the wearer's motion intentions. The regression model is based on the Hill-type musculoskeletal model. Z. Li et al. [29] employed the Hill model to estimate the joint torque and muscle stiffness. The joint torque and muscle stiffness are used to construct adaptive impedance controller in the exoskeleton robot. Although the muscle model has been used in controlling lower limb exoskeleton robot, the body parameters of each wearer are not same, that is the parameters of the muscle model of individuals are different. The parameter identification of the muscle models of different wearers are not considered in the above researches. W. Wang et al. [30] proposed a stochastic particle swarm optimization (SPSO) and conjugate gradient algorithms (CG) based muscle model identification method to improve the accuracy of joint torque estimation of sEMG. Although this method can identify models, the identification accuracy needs to be further improved to provide better control effects.

This paper mainly makes the following contributions to the parameter identification of the Hill model:

1. First, a new parameter identification paradigm is designed based on exoskeleton robot, and the muscle model parameter identification is realized through three steps.
2. An Adam optimization method with varying learning rate is proposed to achieve stable muscle parameter identification on 8 subjects.
3. The estimation error of the proposed method is competitive with that of the State-of-art method.

The organization of this paper is as follows. In Section 2, the proposed paradigm and the muscle model are described in detail. The platform, experiment protocol and results are described in Section 3. The conclusion is summarized in Section 4. Finally, Some analysis and future work of this research are given in Section 5.

2 Methods

In this section, the framework of the proposed method is introduced in detail firstly. Then the Adam optimizer with variable learning rate are described. The modeling process of the knee joint and the Hill muscle model are introduced for easily understanding the effects of the parameters.

2.1 The Framework of the Proposed Method

The framework of our method is shown in Fig. 1. The whole method can be divided into three parts according to the times of information collection. The first part is to collect

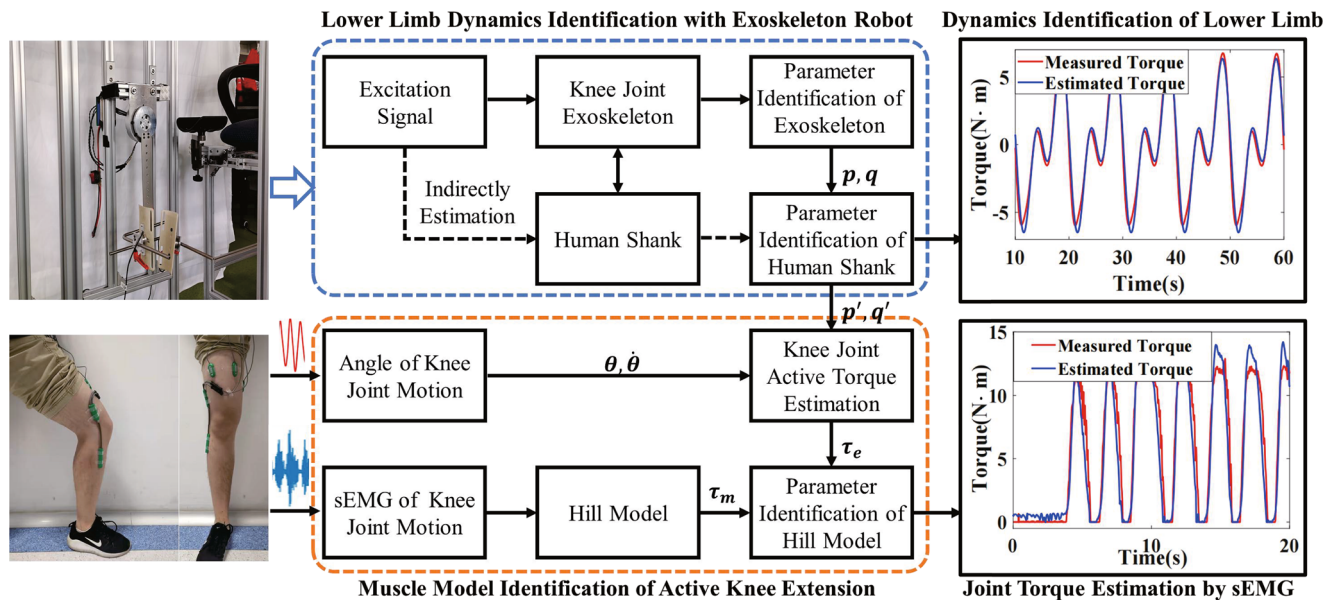


Fig. 1 The framework of the proposed method

the swing angle, angular velocity, and motor torque of the exoskeleton which is unloaded. Then calculate the angular acceleration, and calibrate the dynamic parameters of the exoskeleton (p and q) through model gradient and adam optimization, so as to obtain the exoskeleton kinetic model.

The second part is to collect the swing angle, angular velocity, and motor torque of the exoskeleton under the condition of driving the lower limbs to swing (the subject does not exert force). Then calculate the angular acceleration, and calibrate kinetic parameters (p' and q') of the exoskeleton-lower limb combined model through model gradient and adam optimization, in order to obtain a dynamic model of exoskeleton-lower limb.

At this time, the dynamic parameters and model of the human active force torque (T_{FCE}) can be obtained by making difference of the above two models. Afterwards, the active force torque can be calculated according to the angle and angular acceleration, that is, the indirect measurement value of the active force dynamic torque (\hat{T}_{FCE}) can be obtained.

The last step is to measure the EMG signal when the subject's leg actively swings. Through the hill model, the estimated torque of the knee joint when the lower leg swings is calculated in the forward direction. According to the estimated torque T_{FCE} and the measured torque \hat{T}_{FCE} constructs the optimization target and optimizes the parameters of the hill model by adam optimization.

2.2 Adam Optimizer with Variable Learning Rate

Adaptive moment estimation (Adam) [31] is a very popular training algorithm for deep neural networks, implemented

in many machine learning frameworks. Adam uses a parameter update strategy that is similar to root mean square propagation, but with an added momentum term. It keeps an element-wise moving average of both the parameter gradients and their squared values. In practice the inclusion of momentum often speeds up convergence, but may cause oscillations around the minimum. Hence a variable learning rate strategy is added in the Adam optimizer in this experiment. The variable learning rate η is defined as:

$$\eta = \eta_0 - (\eta_0 - \eta_{end}) \cdot \frac{t}{T} \tag{1}$$

where η_0 is initial learning rate, η_{end} is final learning rate, t is the current number of iteration, and T is the total number of iteration.

2.3 Dynamic Model of Knee Joint

Under the condition that the thigh remains stationary, the movement of the calf around the knee joint is approximately regarded as the rotation of a pendulum rod around the axis. It has only one degree of freedom, like the rotation of a robotic arm. Therefore, dynamic modeling of knee joint movement is conducted. Lagrange method is used to establish the dynamics model, and the model parameters are shown in Table 1.

$$K = \frac{1}{2}m(d\dot{\theta})^2 = \frac{1}{2}md^2\dot{\theta}^2 \tag{2}$$

$$P = mgd \cos \theta \tag{3}$$

Table 1 Lagrangian kinetic parameters

Variable	Expression
lagrange Function	L
Kinetic Energy	K
Potential Energy	P
Torque	τ
Mass	m
Distance from the center of mass to the axis of rotation	d
The Angle of the exoskeleton to the vertical direction	θ

Where g is the acceleration of gravity.

$$L = K - P = \frac{1}{2}md^2\dot{\theta}^2 - mgd \cos \theta \tag{4}$$

$$\frac{\partial L}{\partial \theta} = mgd \sin \theta \tag{5}$$

$$\frac{\partial L}{\partial \dot{\theta}} = \frac{1}{2}md^2(2\dot{\theta}) = md^2\dot{\theta} \tag{6}$$

$$\frac{d}{dt} \cdot \frac{\partial L}{\partial \dot{\theta}} = md^2\ddot{\theta} \tag{7}$$

$$\tau = \frac{d}{dt} \cdot \frac{\partial L}{\partial \dot{\theta}} - \frac{\partial L}{\partial \theta} = md^2\ddot{\theta} - mgd \sin \theta \tag{8}$$

For the same object, m and d are determined. Parameter identification is actually the identification of m and d . However, the direct identification of m and d will cause multiple solutions, and the identification effect is greatly affected by the initial value. Therefore, we set $md^2 = p$, $md = q$, then the dynamic equations of the exoskeleton without load and with load can be expressed as Eqs. 9 and 10 separately.

$$T_e = p\ddot{\theta} - qg \sin \theta \tag{9}$$

$$T_{he} = p'\ddot{\theta} - q'g \sin \theta \tag{10}$$

Where T_e and T_{he} are respectively the output torque of the exoskeleton without load and with load, while p, q and p', q' are respectively the parameters of exoskeleton dynamic equations without load and with load.

In order to train the parameters, whether the exoskeleton is unloaded or loaded, it must swing according to a specific trajectory. The swing we designed is the superposition of two sine waves of different frequencies. This design is to prevent multiple solutions caused by simple swing trajectories. The swing trajectory is shown in Eq. 11:

$$\text{Trace} = C(\sin(0.1 \cdot 2\pi \cdot t) + \sin(0.2 \cdot 2\pi \cdot t)) \tag{11}$$

where C is a fixed constant, and t is time.

Then the dynamic model of human active motion can be obtained by taking the difference between the exoskeleton dynamic model with load and without load.

$$T_{FCE} = T_{he} - T_e = (p' - p) \cdot \ddot{\theta} - (q' - q) \cdot g \cdot \sin \theta \tag{12}$$

Where T_{FCE} is the human active force torque, while T_e and T_{he} have been defined in Eqs. 9 and 10 separately.

Our optimization goal is to minimize the sum of error squares J , which is defined as following:

$$J = \int (\tau - \hat{\tau})^2 \tag{13}$$

where τ is the torque obtained according to the dynamic model, $\hat{\tau}$ is the torque directly measured.

Partial derivatives of the optimization target to the two parameters are shown as Eqs. 14 and 15 respectively.

$$\begin{aligned} \frac{\partial J}{\partial p} &= \frac{\partial J}{\partial \tau} \cdot \frac{\partial \tau}{\partial p} \\ &= 2 \int (\tau - \hat{\tau}) \cdot \ddot{\theta} \end{aligned} \tag{14}$$

$$\begin{aligned} \frac{\partial J}{\partial q} &= \frac{\partial J}{\partial \tau} \cdot \frac{\partial \tau}{\partial q} \\ &= 2 \int (\tau - \hat{\tau}) \cdot (-g \sin \theta) \end{aligned} \tag{15}$$

Once the gradient is calculated, adam can be used for optimization.

2.4 Hill Muscle Model of Active Knee Extension

Hill model is a biomechanical model that describes the function of three-unit skeletal muscle [26, 32]. The contraction element CE is connected in series with a nonlinear elastic element SE , and then in parallel with another nonlinear elastic element PE . According to the hill model, we established a model for solving the joint torque from the EMG signal. There are some parameters in the hill model, and the benchmark values are obtained based on anatomy in the software Opensim, but different individuals have different sexes, so in actual application, the parameters must be optimized.

After the EMG preprocessing, which includes 50Hz notch filtering, 30Hz zero-phase shift high-pass filtering, full-wave rectification, 5Hz zero-phase shift low-pass filtering and normalization in order, the following steps are required to obtain the knee torque from the preprocessed EMG. The neural activation value $u(t)$ is expressed as:

$$u(t) = \alpha e(t - d) - \beta_1 u(t - 1) - \beta_2 u(t - 2) \tag{16}$$

where $u(t), u(t - 1), u(t - 2)$ represent the neural activation values at time $t, t - 1, t - 2$ respectively. $e(t - d)$ represents the EMG signal after preprocessing considering delay time d , which is reported to be between 10 – 100ms. In our study,

fixed $d = 20ms$. To form a stable equation, the following constraints must be satisfied:

$$\begin{aligned} \beta_1 &= \gamma_1 + \gamma_2, & \beta_2 &= \gamma_1\gamma_2, & \alpha - \beta_1 - \beta_2 &= 1, \\ |\gamma_1| &< 1, & |\gamma_2| &< 1 \end{aligned} \tag{17}$$

where α, β_1, β_2 are second order kinetic coefficients. In our study, fixed $\gamma_1 = \gamma_2 = 0.5$, therefore $\beta_1 = 1.0, \beta_2 = 0.25, \alpha = 2.25$. The muscle activation value $a(u)$ is denoted as:

$$a(u) = \frac{e^{AuR^{-1}} - 1}{e^A - 1} \tag{18}$$

where A is the nonlinear shape factor that defines the curvature of the function, satisfying $A \in [-3, 0]$, R is the maximum neural activation in MVC(maximum random contraction), which is defined as follows:

$$R = k_r u_{\max} \tag{19}$$

where u_{\max} is the maximum value of neural activation, k_r is a ratio to be optimized. The optimal fiber length l_o^m is expressed as:

$$l_o^m = l_o(\lambda(a(u) - 1) + 1) \tag{20}$$

where l_o is the optimal muscle fiber length at zero activation, $a(u)$ is the muscle activation value, λ is the parameter to be optimized.

The normalized fiber length \tilde{l}^m is expressed as:

$$\tilde{l}^m = \frac{l^m}{l_o^m} \tag{21}$$

where l^m is the actual fiber length, which will change with motion.

$$l^m = k_s l_f^m \tag{22}$$

where l_f^m is the data obtained by opensim fitting, and k_s is the parameter to be optimized. In the opensim model gait2392, l_f^m has an approximate linear relationship with the change of the knee joint angle. Therefore, we use linear fitting to obtain the relationship between l_f^m and the joint angle.

Muscle fiber length influence factor F_{l-f} shows how F_{CE} is affected by muscle fiber length. In the process of muscle contraction, the length of muscle fiber changes constantly, resulting in the change of the main force. With the gradual increase of the length of muscle fiber, the main force shows a trend of first increase and then decrease. When the muscle fiber reaches the optimal length of muscle fiber, the main force of muscle fiber reaches the maximum at this time.

$$f_{l-f} = e^{-\frac{(\tilde{l}^m - 1)^2}{\gamma}} \tag{23}$$

where γ is the active force-length relationship shape factor, usually 0.45, which is related to age. The normalized fiber motion velocity \tilde{v}^m is expressed as:

$$\tilde{v}^m = \frac{v^m}{v_{\max}} \tag{24}$$

where v^m is the actual shrinkage speed of the fiber [33], which satisfies $v^m = -\dot{l}^m$, because \dot{l}^m is l^m Changes in elongation rather than shrinkage. As mentioned earlier, in our research, l^m is linearly fitted with angle, so v^m is obtained by linear fitting with angular velocity. v_{\max} is the maximum contraction speed of muscle fibers, which satisfies $v_{\max} = 10l_o k_v$, where l_o is the same as before, and k_v is the parameter to be optimized.

The muscle force increases with the increase of muscle fiber contraction speed. When the muscle fiber reaches the ideal contraction speed, the main force of the muscle fiber is about 1.5 times that of the maximum isometric or contraction state. Influence factor of muscle fiber contraction velocity F_{v-f} is represented as:

$$f_{v-f} = \begin{cases} \frac{1 + \tilde{v}^m}{1 - \frac{\tilde{v}^m}{A_{fv}}}, & \tilde{v}^m \leq 0 \\ \frac{g_{\max} \cdot \tilde{v}^m + \frac{A_{fv}(g_{\max}-1)}{A_{fv}+1}}{\tilde{v}^m + \frac{A_{fv}(g_{\max}-1)}{A_{fv}+1}}, & \tilde{v}^m > 0 \end{cases} \tag{25}$$

where g_{\max} is the maximum normalized muscle elongation force, with a value of 1.5. A_{fv} is the factor of the hill model, and the value is 0.25.

The active muscle force is expressed as:

$$F_{CE} = a \cdot f_{l-f} \cdot f_{v-f} \cdot F_0^M \tag{26}$$

where, a is the muscle activation; f_{l-f} is the influence factor of muscle fiber length; f_{v-f} is the influence factor of muscle fiber contraction speed; F_0^M is the maximum isometric contraction force of muscle fiber, which can be obtained directly from Opensim. According to the above formula, F_{CE} can be expressed in detail as:

$$F_{CE} = \begin{cases} a \cdot e^{-\frac{(\tilde{l}^m - 1)^2}{\gamma}} \cdot \frac{1 + \tilde{v}^m}{1 - \frac{\tilde{v}^m}{A_{fv}}} \cdot F_0^M & v_f \leq 0 \\ a \cdot e^{-\frac{(\tilde{l}^m - 1)^2}{\gamma}} \cdot \frac{g_{\max} \cdot \tilde{v}^m + \frac{A_{fv}(g_{\max}-1)}{A_{fv}+1}}{\tilde{v}^m + \frac{A_{fv}(g_{\max}-1)}{A_{fv}+1}} \cdot F_0^M & v_f > 0 \end{cases} \tag{27}$$

The feathery characteristics of human skeletal muscles indicate that there is a certain angle between the force generated by muscle fibers and the force acting on the bone, that is, the pinnate angle, and the effect of the pinnate angle on the output force of muscle fibers cannot be ignored. When the muscle fiber is in a resting state, the muscle thickness h can be expressed as:

$$h = l_0 \cdot \sin \varphi_0 \tag{28}$$

When the muscle fiber is in any position, the muscle thickness h satisfies:

$$h = l^m \cdot \sin \varphi \tag{29}$$

Then the pinnate angle φ corresponding to different muscle fiber lengths can be obtained:

$$\varphi = \arcsin\left(\frac{l_0 \sin \varphi_0}{l^m}\right) \tag{30}$$

where l_0 is the length of the muscle fiber in the resting state, φ_0 is the pinnate angle in the resting state, l^m is the length of the muscle fiber at any time. Muscle force F_M is expressed as:

$$F_M = F_T = F_f \cdot \cos \varphi = (F_{CE} + F_{PEE}) \cdot \cos \varphi \tag{31}$$

where F_{CE} is the active force of muscle fiber; F_{PEE} is the negative force of muscle fiber [34]. Since this research focuses on the active muscle force generated by the EMG signal, the muscle force in this paper is expressed as:

$$F_{MCE} = F_{CE} \cdot \cos \varphi \tag{32}$$

For a specific muscle i , its force arm r_i is expressed as:

$$r_i = \partial l_i^{mt} / \partial \theta \tag{33}$$

where l_i^{mt} refers to the sum of muscle length and tendon length of a specific muscle i rather than the length of individual muscle fibers. l_i^{mt} satisfies:

$$l_i^{mt} = l_i^m \cos \varphi_i + l_i^t \tag{34}$$

where l_i^t is the tendon length, which changes very little during muscle exercise. Therefore, it is considered to be a constant value in this study, so r_i can be expressed as:

$$\begin{aligned} r_i &= \frac{\partial l_i^{mt}}{\partial \theta} \\ &= \frac{\partial (l_i^m \cos \varphi_i)}{\partial \theta} \\ &= \frac{\partial l_i^m}{\partial \theta} \cos \varphi_i + l_i^m \frac{\partial \cos \varphi_i}{\partial \theta} \\ &= \frac{\partial l_i^m}{\partial \theta} \cos \varphi_i + l_i^m \frac{\partial \cos \varphi_i}{\partial \varphi_i} \cdot \frac{\partial \varphi_i}{\partial l_i^m} \cdot \frac{\partial l_i^m}{\partial \theta} \\ &= \frac{\partial l_i^m}{\partial \theta} (\cos \varphi_i + l_i^m \cdot (-\sin \varphi_i) \cdot \frac{\partial \varphi_i}{\partial l_i^m}) \end{aligned} \tag{35}$$

Set the part in parentheses in Eq. 30 as K , we can get:

$$\begin{aligned} \frac{\partial \varphi_i}{\partial l_i^m} &= \frac{\partial \varphi_i}{\partial K} \cdot \frac{\partial K}{\partial l_i^m} \\ &= \frac{1}{\sqrt{1-K^2}} \cdot \frac{-l_0^i \sin \varphi_0^i}{(l_i^m)^2} \end{aligned} \tag{36}$$

So r_i can be expressed as:

$$r_i = \frac{\partial l_i^m}{\partial \theta} \left(\cos \varphi_i + \frac{\sin \varphi_i \cdot l_0^i \cdot \sin \varphi_0^i}{l_i^m \cdot \sqrt{1-K^2}} \right) \tag{37}$$

The above is the calculation of the torque of single muscle. In this study, the active force torque of the knee joint is regarded as the sum of 3 muscles, so the active force torque T_{FCE} is expressed as:

$$T_{FCE} = \sum_{i=1}^3 r_i F_i^{MCE} \tag{38}$$

3 Experiments

In this section, the exoskeleton platform and the experiments protocol are described at first. Then three experimental results are introduced in detail to evaluate the performance of the proposed method. We selected a total of eight subjects. Their age is 23.8750 ± 0.8345 years old, their height is 173.8750 ± 5.6930 cm, and their weight is 65.5000 ± 7.0912 kg.

3.1 Platform

The experimental platform is shown in Fig. 2. Subjects sit on a special experimental chair, with their right thigh held up by the support frame, which kept them basically level. The right shank wears an exoskeleton. The exoskeleton is fixed in the frame by bolt links, and the position can be adjusted front and back while up and down to adapt to different subjects, in order to make the rotation axis of the knee joint maintain consistency with the rotation axis of the exoskeleton motor. The drive is a high-performance DC servo drive (Accelnet AEM-090-30), and realizes the position, speed and torque control of the motor through the Ethernet fieldbus EtherCAT. The driving motor is a DC servo motor (HT-03), which is matched with a reducer with a reduction ratio of 6:1, and the maximum output torque is $17N \cdot m$, which can drive the subjects' shanks to swing.

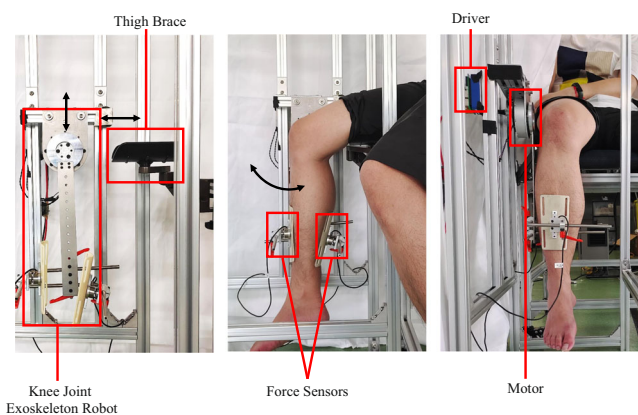
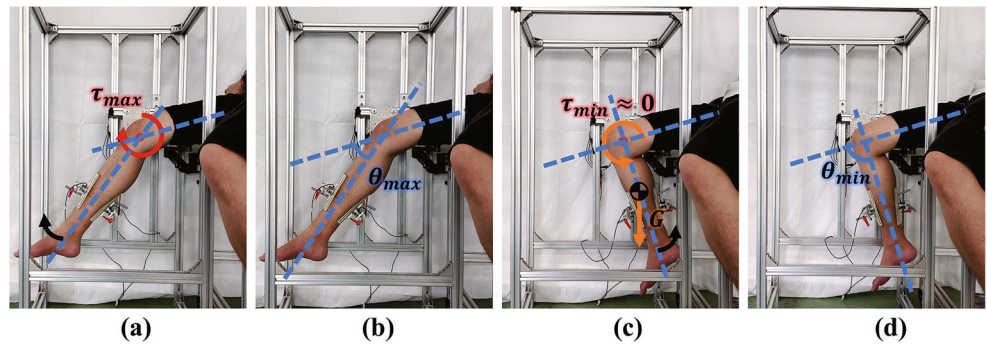


Fig. 2 Experiment platform

Fig. 3 Motion process of the subject. (a) represents $\theta > \theta_0$ and swing forward; (b) represents $\theta > \theta_0$ and swing backward; (c) represents $\theta < \theta_0$ and swing backward; (d) represents $\theta < \theta_0$ and swing forward



3.2 Experiments Protocol

As mentioned in Eq. 33, the angle between the shank and the thigh is θ . The knee joint exercises include stretching exercises and knee bending exercises, which correspond to the forward and backward swing of the calf respectively. When the leg is straight, $\theta = 0$. According to the definition standard of opensim, θ decreases during knee bending, and θ increases during stretching, so the range of θ is defined as $-120^\circ \sim 0^\circ$. The form of exercise aimed at in this study is that, the subject sits on a chair with the right thigh lifted to remains basically level during the experiment, and the lower leg is suspended and can swing freely.

When at rest, the subject's leg is relaxed, and the lower leg is naturally perpendicular to the ground. At this time, $\theta = \theta_0$. Generally speaking, the thigh can not be completely

horizontal, but slightly inclined downward, so θ_0 is often slightly larger than -90° , around -85° . Based on the size relationship between θ and θ_0 and the difference in the direction of movement, the movement is divided into 4 processes, as shown in Fig. 3. The movement continues in the order of (a) \rightarrow (b) \rightarrow (c) \rightarrow (d) \rightarrow (a) \rightarrow (b) \rightarrow (c) \rightarrow (d)..., which constitutes the periodic swing of the shank. In the processes a and b, it is the quadriceps that drives the knee joint to drive the shank.

In process (a), the quadriceps muscle needs to work against gravity and generate the acceleration of the lower leg. In this process, overcoming gravity is the main task, because the acceleration of motion is not great. Therefore, in this process, the torque generated by the quadriceps muscle increases continuously, and when the motion angle reaches the extreme value, the torque also basically reaches the extreme value. In process (b), gravity and the quadriceps muscle work together to generate acceleration of motion, and the quadriceps muscle contraction decreases, resulting in a decreasing torque.

As can be seen in Fig. 4, the rectus femoris, lateral femoris, and medial femoris muscles are close to the human epidermis, so their surface electromyography is easy to collect. The intermediary femoris muscle is located on the deep surface of the rectus femoris and is covered by the rectus femoris. Therefore, its EMG signal is difficult to collect without injury. Therefore, this study only collected

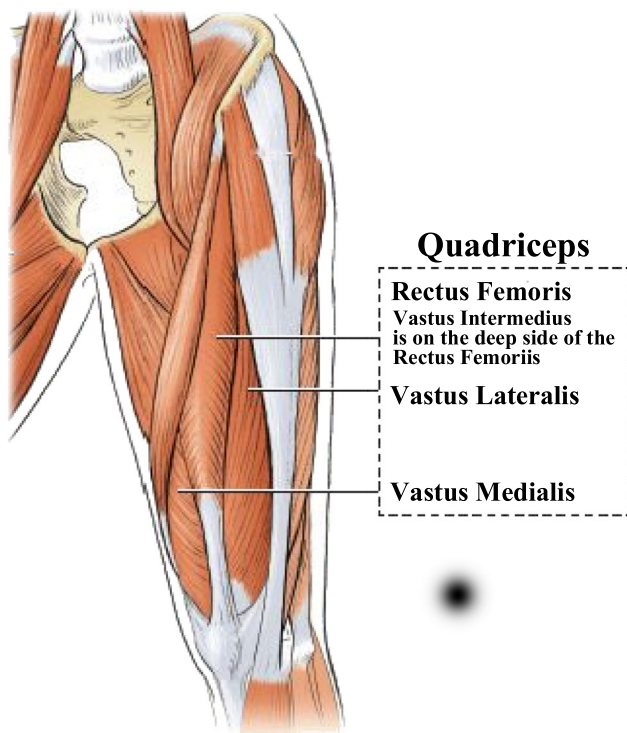
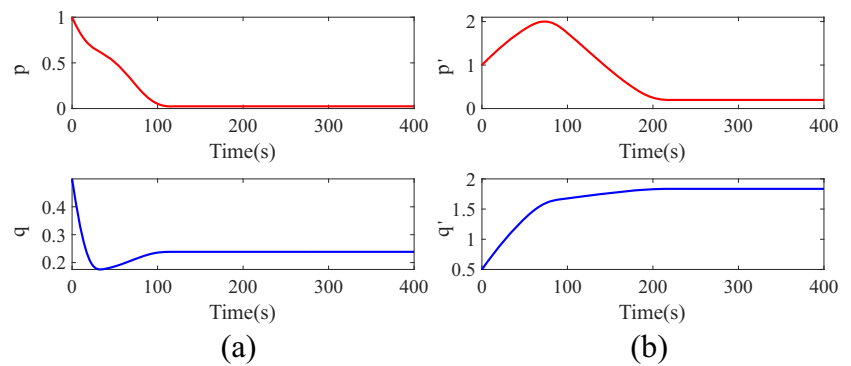


Fig. 4 The quadriceps

Table 2 Dynamic parameters of exoskeleton in different states

Pattern	$p(p')$	$q(q')$
Empty	0.0244	0.2385
Hold Subject 1	0.0819	1.4886
Hold Subject 2	0.0089	1.6919
Hold Subject 3	0.1983	1.8353
Hold Subject 4	0.0690	1.5165
Hold Subject 5	0.0740	1.4845
Hold Subject 6	0.1553	1.8205
Hold Subject 7	0.1446	1.5388
Hold Subject 8	0.1325	1.7929

Fig. 5 Convergence process of dynamic parameters. (a) represents the convergence process of the dynamic parameters of the exoskeleton without load; (b) represents the convergence process of the dynamic parameters of the exoskeleton driving the shank



the EMG signals of the rectus femoris, lateral femoris and medial femoris to estimate the main dynamic torque of the knee joint. The role of the intermediate femoris muscle will be compensated in the parameter optimization.

3.3 Parameters Convergence Process

It can be seen from the Table 2 and Fig. 5 that the value of parameter p is much smaller than q whether it is no-load or load. According to our setting, $p = md^2$, $q = md$. The length of the exoskeleton is about $0.3m$, and the average length of the shanks of the 8 subjects is about $0.4m$. Assuming that their center of gravity is at the midpoint, for the unloaded exoskeleton, $d = 0.15m$; for the loaded exoskeleton, $d < 0.2m$. That is, p is one order of magnitude smaller than q , and the experimental results meet the hypothesis. It can be seen from Eq. 11 that the swing frequency is low and the acceleration is not large. In the dynamic model, p represents the role played by acceleration, and q represents the role played by gravity. Therefore, we show from the theoretical and experimental results that in the movement paradigm we designed, the torque generated by the exoskeleton and human legs to overcome gravity plays a major role, and the torque generated by the acceleration plays a secondary role. Therefore, it can be considered that the active force dynamics model we established is relatively reliable.

It can be seen from Fig. 6 that the dynamic parameters of the exoskeleton have a good regression effect no matter it is unloaded or loaded. The deviation of the regression mainly appears near the extreme point. When loaded, the error is slightly larger than that of no-load. The reason is that certain relative motion and friction will occur in the interaction between human and exoskeleton, which we ignore in the modeling because we think it is not important. However, it will still be reflected in the results. It can also be found from Fig. 5 that the dynamic parameters of the unloaded exoskeleton achieve good convergence around 100s, while the dynamic parameters of the loaded exoskeleton achieve good convergence around 200s. The reason is also the same, that is, for the model with load, some minor items are ignored, making the error between it and the actual dynamic model larger than that of the unloaded model. But even so, the error is still within an acceptable range.

It can be seen from Fig. 7 that the convergence speed of different parameters is different. It can be sorted according to the speed of convergence: k_r , A , λ , k_s , k_v . It can also be seen from Fig. 7 and Table 3 that the parameter convergence process and results of different subjects are relatively consistent, but there are also some differences. For the parameters A , k_r , λ , the convergence results of different subjects are relatively close; for the parameters k_s , k_v , the convergence results of different subjects are somewhat different. The more unique one is Subject 3.

Fig. 6 Torque in motion of the exoskeleton. (a) is the regression result of torque when the exoskeleton is unloaded; (b) represents the regression result of torque when the exoskeleton is loaded

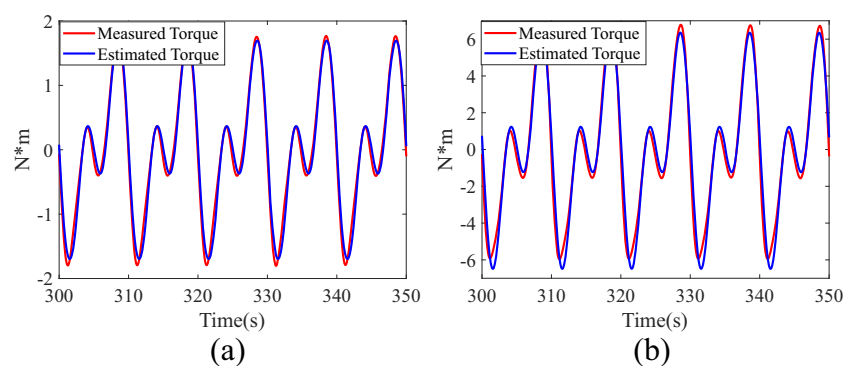
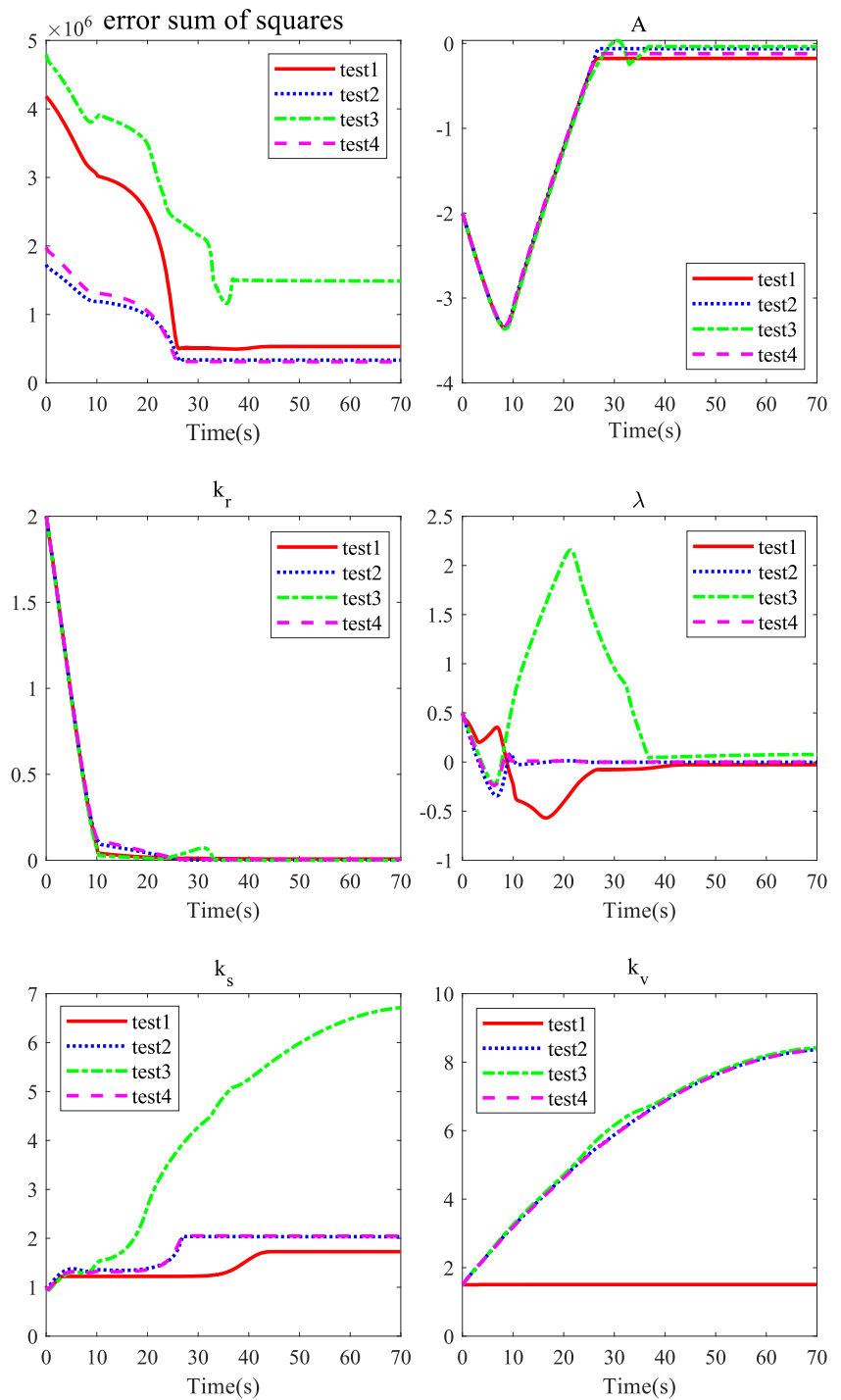


Fig. 7 Convergence process of hill model parameters of four subjects (subjects 1 to 4)



The mean square error of his torque regression is larger than that of the other three subjects. At the same time, his parameters generally converge more slowly than the other three subjects. The final convergence value of parameter k_s differs greatly from that of the other three subjects. In our experiment, all parameters will be updated in each step of iteration. The different convergence speeds of parameters give us some enlightenment. In the following research, we

will try to fix some parameters and let others converge first to explore the influence of different parameter convergence orders on the results.

3.4 Torque Estimation Results

There are two main differences between the torque of Figs. 8 and 9. First, Fig. 8 shows the training process, while

Table 3 Hill Model Parameter Convergence Results of 8 Subjects

Subject	A	k_r	λ	k_s	k_v
Subject1	-0.1759	0.0076	-0.0274	1.7264	1.5069
Subject2	-0.0622	0.0024	-0.0024	2.0329	8.3654
Subject3	-0.0375	0.0006	0.0773	6.7156	8.4225
Subject4	-0.1211	0.0046	-0.0002	2.0457	8.3562
Subject5	-0.0478	0.0012	0.0841	6.8002	1.4989
Subject6	-0.0275	0.0007	-0.0005	2.3908	8.4695
Subject7	-0.0137	0.0003	0.0224	7.1072	8.2168
Subject8	-0.0377	0.0010	-0.0016	2.3500	8.3705

Fig. 9 shows the final convergence result. Second, Fig. 9 deletes the torque less than 0. This is because the muscles selected by us locate in the front of the thigh (Fig. 4). In addition, we divide the leg swing into four consecutive periodic stages (Fig. 3). In the (a) and (b) stages of Fig. 3, the three muscles (RF, VL and VM) selected in this paper provide the torque of knee joint movement; in the (c) and (d) stages of Fig. 3, these three muscles are basically in a resting state, and the torque of knee joint movement is provided by the muscles at the back of the thigh, which is not the research content of this paper.

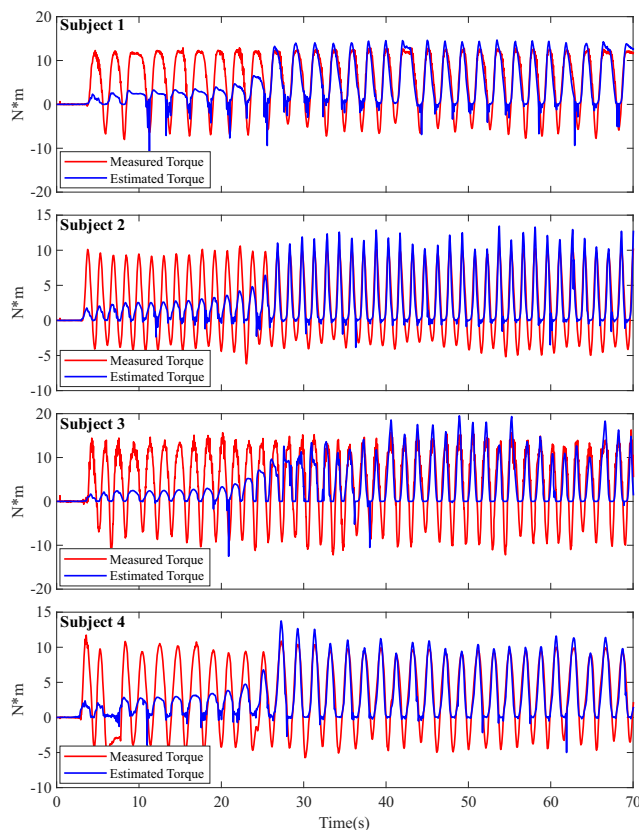


Fig. 8 Torque convergence process of 4 subjects

In Figs. 8 and 9, the measured torque (red line) is calculated by the dynamic model described in Section 2.3, which expressed the knee joint output torque, while the estimated torque (blue line) is estimated from the EMG signal based on the hill model.

In Fig. 9, we mark the EMG cycle and the torque cycle in the same time period with the same color rectangular box, and use a different color to distinguish the adjacent cycle. By comparing any period of EMG signal and the change of torque in the corresponding period, it can be found that when the EMG signal is output, that is, when the three muscles are active, both the measured torque (red line) and the estimated torque (blue line) are positive, corresponding to the stage (a) and (b) in Fig. 3. When the EMG signal is near 0, that is, when the three muscles are resting, the measured torque (red line) should be negative and the estimated torque (blue line) should be 0, corresponding to the (c) and (d) stages in Fig. 3.

This means that not all points have to be calculated in the training process to make estimated torque (blue line) fit the measured torque (red line). Because in each cycle, there is a period of time when there is no output signal from the EMG. During this period, the estimated torque (blue line) from the EMG is 0, and the measured torque (red line) from the dynamic equation is negative. But in practice, we didn't simply train for periods of time when the measured torque was positive. First, the training process would not be continuous if we did it, because we had to break up a series of successive swing periods. Second, we wanted to test whether the model would overfit during the training, since we didn't limit the range of the force arm in (33).

Therefore, when training the model, we used all the torque data during exercise, instead of just taking data greater than 0. It can be seen from Fig. 8 that during the entire training process, the measured torque (red line) alternates between positive and negative, and the estimated torque (blue line) generally stops to fall when it drops to 0, and it will be less than 0 on rare occasions. This is the overfitting situation of training. But overall the training effect is good.

From the foregoing, when estimating the error, in the interval where the EMG is 0, the estimated torque (blue line) should be 0, and the measured torque (red line) is negative. It is meaningless to calculate the estimated error in these intervals. Therefore, in Fig. 9, the part where the torque is less than 0 is uniformly truncated to show the training effect more clearly. After that, the estimation error is calculated.

It can also be seen that the motion frequencies of the eight subjects are not exactly the same, and the motion frequency of Subject 2 is obviously higher than that of the other subjects. From Fig. 9 we can see that in the period of 20s – 50s, subject 2 moved about 20 cycle, and subject 4 moved about 12 cycles. It can be found that the estimated

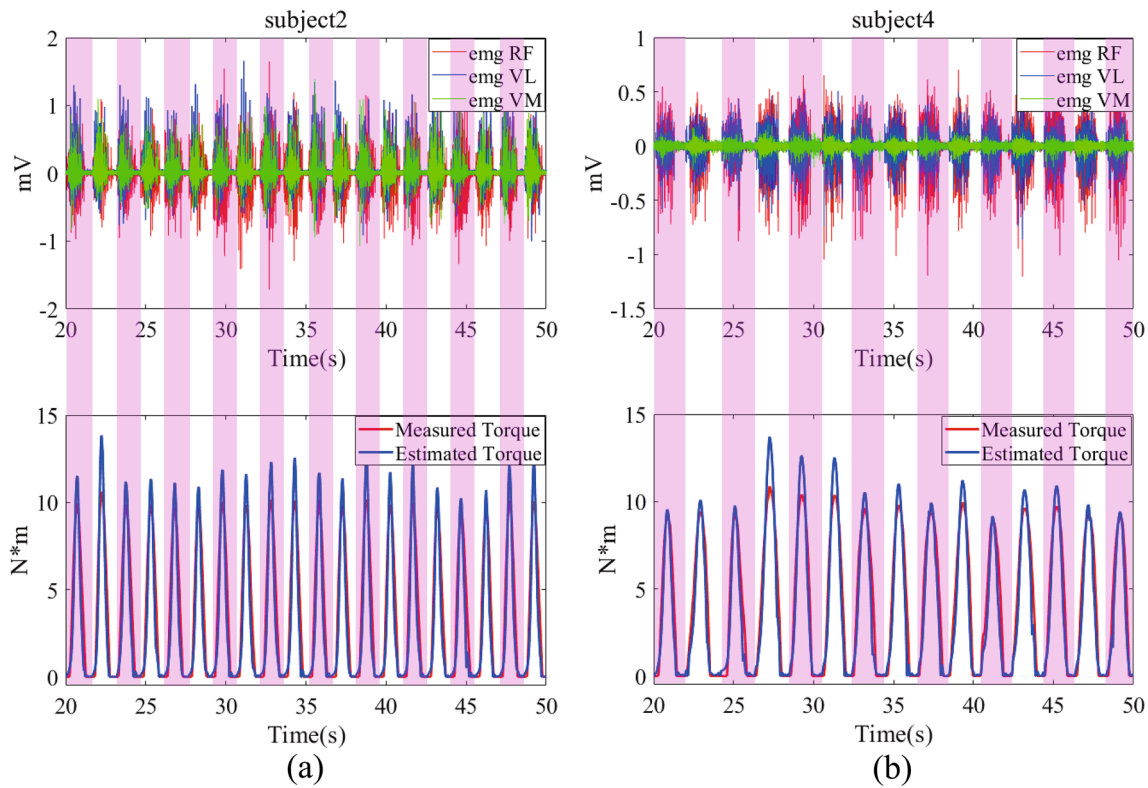


Fig. 9 Torque convergence results of 2 Subjects. (a) is the original EMG value of the three muscles and the hill model based final torque convergence result of subject2; (b) is the original EMG value of the three muscles and the hill model based final torque convergence result of subject4

torque of subject 2 is larger than the calculated torque near the peak; and the estimated torque of subject4 is closer to the calculated torque near the peak. The reason is as mentioned above. In the process of establishing the dynamic model of the active force of the knee joint, the swing velocity and the acceleration is small, while the friction and other items are ignored. But in fact these factors are reflected in the autonomous swing.

It can be seen from the Table 4 that the RMSE, MAXE, and MAE sizes of different subjects are correlated. Among them, the error of subject 3 is significantly different from

Table 4 Torque estimation error of 8 subjects

Subject	RMSE	MAXE	MAE
Subject 1	1.7088	5.8500	0.9887
Subject 2	1.2635	5.3161	0.6872
Subject 3	2.7036	11.5735	1.4628
Subject 4	1.1108	4.8781	0.6081
Subject 5	1.6819	8.4163	1.0952
Subject 6	1.7834	7.9022	1.2019
Subject 7	2.0501	6.4855	1.2532
Subject 8	2.3667	7.5066	1.5866
mean	1.8336	7.2411	1.2445

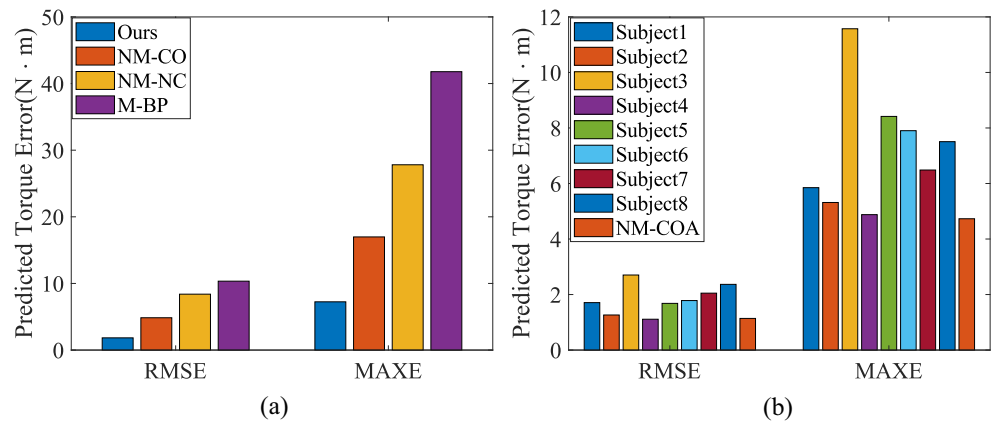
the errors of the other subjects. The MAXE of the others are all less than 8; while the MAXE of subject 3 is greater than 11. The RMSE of subject 3 is also greater than others. The reason is as mentioned above, the convergence effect of subject 3 is not as good as that of the other subjects.

It can be seen in Table 5 and Fig. 10(a) that the average values of RMSE and MAXE of the eight subjects are significantly smaller than the NM-CO, NM-NC and M-BP methods [30]. As shown in Fig. 10(b), compared with NM-COA, only subject 4’s RMSE is smaller than its value (1.1108 vs. 1.14), but the other seven subjects’ RMSE is larger than it. The MAXE of the eight subjects are all larger than NM-COA’s value. In detail, subject 4’s value is very close to it(4.8781 vs. 4.73), and the MAXEs of the other seven subjects are slightly farther away from it. Although

Table 5 Torque estimation error of different models

method	RMSE	MAXE
ours	1.8336	7.2411
NM-CO	4.85	16.98
NM-COA	1.14	4.73
NM-NC	8.39	27.81
M-BP	10.34	41.78

Fig. 10 Bar diagram of torque estimation error. (a) is the comparison between the average RMSE and MAXE values of 8 subjects obtained by our method and the results of methods NM-CO, NM-NC and M-BP; (b) is the comparison between RMSE and MAXE of 8 subjects obtained by our method and method NM-COA



the performance of torque prediction is comparable with NM-COA, the proposed method have few parameters and the times of iteration of the gradient based method (Our method) is less than the heuristic based algorithm (NM-COA).

3.5 The Effects of Variable Learning Rate in Adam Optimizer

It can be seen from Fig. 11 that under a fixed learning rate, the parameters will not converge to a fixed value, and will eventually oscillate around the value; while under a variable learning rate, the parameters will eventually converge to

a fixed value. Under a fixed learning rate, the time for parameter convergence is relatively short. In Fig. 11(a), A converges around 15s, while in Fig. 11(b) A converges around 30s. The reason is that the variable learning rate is reduced during iteration, and therefore converges more and more slowly.

4 Conclusion

To overcome the shortcoming of identifying the Hill muscle model with experience, a three-step parameter identification paradigm is designed for accurately identifying the param-

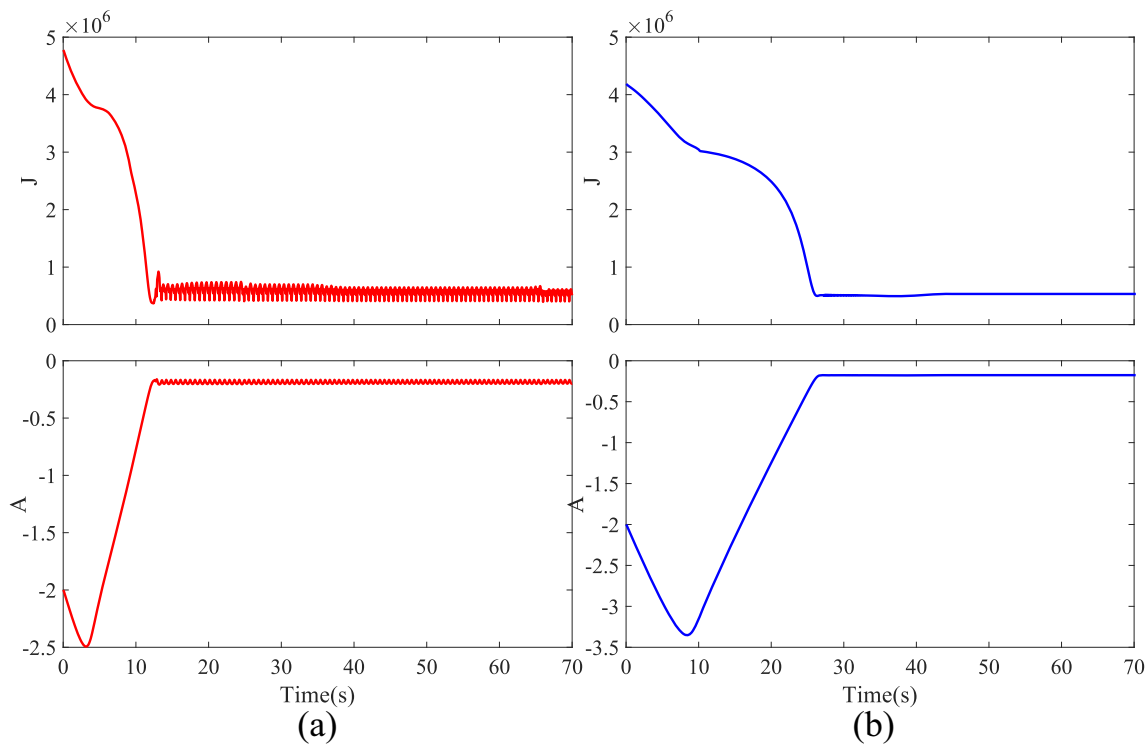


Fig. 11 Fixed learning rate versus variable learning rate. (a) is the convergence process of mean square error and parameter A under fixed learning rate; (b) is the convergence process of mean square error and parameter A under variable learning rate

eters of muscle model. The exoskeleton robot is employed in the identification process to estimate the kinetic parameters of human limb. The adam optimizer with variable learning rate is employed in the Hill model identification. The optimizer with variable learning rate shows good convergence performance comparing to the with fixed learning rate optimizer. The identified Hill muscle model have lower torque prediction error than the NM-CO, NM-NC and M-BP based methods. The performance of the proposed method is competitive with that of the State-of-art method.

5 Discussion and Future Work

From our results, it can be seen that by optimizing the parameters of the hill model, the active force torque of the knee joint estimated by emg can be very close to that calculated by the dynamic model. But it should be pointed out that we only optimized some of the parameters, and took fixed values for other parameters, such as the EMG delay d in Eq. 16. Because in the definition of the model, its gradient cannot be described, so gradient descent related algorithms cannot be used. In the next step, we plan to use heuristic algorithms to achieve higher model identification accuracy. Another point is that in the process of dynamic parameter identification, although we used harmonics to increase the complexity of the trajectory, the motion trajectory was still at a fixed and low frequency. Therefore, the estimated dynamic model is not good enough to adapt to higher speed motions. In the next step, we will increase the complexity of the trajectory to achieve better dynamic parameter identification, thereby laying a better foundation for hill model parameter identification.

Author Contributions Pengchen Lian: Conceptualization, Methodology, Software, Validation, Writing - original draft Yue Ma: Discussion, Supervision, Methodology, Validation, Writing - review & editing Liangsheng Zheng: Discussion, Hardware Yang Xiao: Discussion, Hardware Xinyu Wu: Discussion, Funding acquisition, Supervision, Writing - review

Funding The work described in this paper is partially supported by International Science & Technology Cooperation Program of China (2018YFE0125600), National Natural Science Foundation of China (Grants No. 62125307, Grant No. 62103401, Grant No. U2013209), NSFC-Shenzhen Robotics Research Center Project (U2013207) and China Postdoctoral Science Foundation (No. 2021M693314).

Declarations

Consent to participate All of the authors declare the consent to participate in this manuscript.

Consent for Publication All of the authors declare the consent to publish this manuscript.


Conflict of interests The authors have no conflicts of interest to declare that are relevant to the content of this article.

References

- Meijneke, C., Oort, G.V., Sluiter, V., Asseldonk, E.V., Tagliamonte, N.L., Tamburella, F., Pisotta, I., Masciullo, M., Arquilla, M., Molinari, M., Wu, A.R., Dzeladini, F., Ijspeert, A.J., Kooij, H.V.D.: Symbitron exoskeleton: Design Control, and Evaluation of a Modular Exoskeleton for Incomplete and Complete Spinal Cord Injured Individuals. In: IEEE Transactions on Neural Systems and Rehabilitation Engineering, vol. 29, pp. 330–339 (2021)
- Wang, T., Zhu, Y., Zheng, T., Sui, D., Zhao, S., Zhao, J.: PALExo: A Parallel Actuated Lower Limb Exoskeleton for High-Load Carrying. IEEE Access **8**, 67250–67262 (2020)
- Wu, X., Ma, Y., Yong, X., Wang, C., He, Y., Li, N.: Locomotion mode identification and gait phase estimation for exoskeletons during continuous multilocomotion tasks. IEEE Trans. Cogn. Develop. Syst. **13**(1), 45–56 (2021)
- Cao, W., Chen, C., Wang, D., Wu, X., Chen, L., Xu, T., Liu, J.: A Lower Limb Exoskeleton with Rigid and Soft Structure for Loaded Walking Assistance. IEEE Robotics and Automation Letters, vol. 7, no. 1, pp. 454–461 Jan. (2022)
- Liu, J., He, Y., Yang, J., Cao, W., Wu, X.: Design and analysis of a novel 12-DOF self-balancing lower extremity exoskeleton for walking assistance. Mech. Mach. Theory **167**, 104519 (2022)
- Ma, Y., Wu, X., Yi, C., Wang, C., Chen, C.: A Review on human-exoskeleton coordination towards lower limb robotic exoskeleton systems. Int. J. Robot. Autom. **34**(4), 431–451 (2019)
- Jang, J., Kim, K., Lee, J., Lim, B., Cho, J., Shim, Y.: Preliminary study of online gait recognizer for lower limb exoskeletons, 2017 IEEE/RSJ International Conference on Intelligent Robots and Systems (IROS), 24–28 Sept., Vancouver, BC, Canada, pp. 5818–5824 (2017)
- Liu, L., Leonhardt, S., Ngo, C., Misgeld, B.J.E.: Impedance-controlled variable stiffness actuator for lower limb robot applications. IEEE Trans. Autom. Sci. Eng. **17**(2), 991–1004 (2020)
- Li, M., Deng, J., Zha, F., Qiu, S., Wang, X., Chen, F.: Towards online estimation of human joint muscular torque with a lower limb exoskeleton robot. Applied Science **2018**(8), 1610 (2018)
- Gordileeva, S.Yu., Lobov, S.A., Grigorev, N.A., Savosenkov, A.O., Shamshin, M.O., Lukoyanov, M.V., Khoruzhko, M.A., Kazantsev, V.B.: Real-time EEG-EMG human-machine interface-based control system for a lower-limb exoskeleton. IEEE Access **8**, 84070 (2020)
- Abusedra, L.F., Busedra, H.F., Elzawi, M.: Lower limb exoskeleton control using EMG signal analysis. In: Proceedings of the 6th international conference on engineering & MIS (2020)
- Ma, Y., Wu, X., Yang, S.X., Dang, C., Liu, D., Wang, C., Wang, C., Chen, C.: Online gait planning of Lower-Limb exoskeleton robot for paraplegic rehabilitation considering weight transfer process. IEEE Trans. Autom. Sci. Eng. **18**(2), 414–425 (2021)
- Lopes, J.M., Figueiredo, J., Pinheiro, C., Reis, L.P., Santos, C.P.: Biomechanical assessment of adapting trajectory and human-robot interaction stiffness in impedance-controlled ankle orthosis. J. Intell. Robot. Syst. **102**(2021), 76 (2021)
- Llorente-Vidrio, D., Lázaro, R.P., Ballesteros, M., Salgado, I., Cruz-Ortiz, D., Chairez, I.: event driven sliding mode control of a lower limb exoskeleton based on a continuous neural network Electromyographic signal classifier. Mechatronics **72**(2020), 102451 (2020)
- Zhang, L., Ma, Y., Wang, C., Yan, Z., Wu, X.: A Method for arm motions classification and a lower-limb exoskeleton control based on sEMG signals, 2019 IEEE 4th International Conference

- on Advanced Robotics and Mechatronics (ICARM), 3-5 July, Toyonaka, Japan, pp. 118-123 (2019)
16. Liu, H.J., Young, K.Y.: Upper-limb EMG-based robot motion governing using empirical mode decomposition and adaptive neural fuzzy inference system. *J Intell. Robot. Syst.* Vol. **68**(2012), 275–291 (2012)
 17. Li, Z., Wang, B., Sun, F., Yang, C., Xie, Q., Zhang, W.: sEMG-based joint force control for an upper-limb power-assist exoskeleton robot. *IEEE J. Biomed. Health Inform.* **18**, 3 (2014)
 18. Kiguchi, K., Hayashi, Y.: An EMG-based control for an upper-limb power-assist exoskeleton robot. *Trans Syst Man Cybern B Cybern* **42**, 4 (2012)
 19. Gui, K., Tan, U.-X., Liu, H., Zhang, D.: Electromyography-driven progressive assist-as-needed control for lower limb exoskeleton. *IEEE Trans. Med. Robot. Bionics* **2**, 1 (2020)
 20. Yin, G., Zhang, X., Chen, D., Li, H., Chen, J., Chen, C., Lemos, S.: Processing surface EMG signals for exoskeleton motion control. *Frontiers in Neurorobotics* **14**, 40 (2020)
 21. Peng, L., Hou, Z.-G., Kasabov, N., Hu, J., Peng, L., Wang, W.-Q.: sEMG-based Torque Estimation for Robot-Assisted Lower Limb Rehabilitation International Joint Conference on Neural Networks (IJCNN), 12-17 July, Killarney, Ireland (2015)
 22. Ma, X., Long, X., Yan, Z., Wang, C., Guo, Z., Wu, X.: Real-time Active Control of a Lower Limb Exoskeleton Based on sEMG. In: Proceedings of the IEEE/ASME International Conference on Advanced Intelligent Mechatronics (AIM), July 8-12, Hong Kong, China (2019)
 23. Su, C., Chen, S., Jiang, H., Chen, Y.: Ankle joint torque prediction based on surface Electromyographic and angular velocity signals. *IEEE Access* **8**, 217681 (2020)
 24. Xia, L., Feng, Y., Chen, F., Wu, X.: A bio-signal enhanced adaptive impedance controller for lower limb exoskeleton, IEEE International Conference on Robotics and Automation (ICRA), 31 May-31 August, Paris, France (2020)
 25. Khoshdel, V., Akbarzadeh, A., Naghavi, N., Sharifnezhad, A., Souzanchi-Kashani, M.: SEMG-based impedance control for lower-limb rehabilitation robot. *Intell. Serv. Robot.* **11**(2018), 97–108 (2018)
 26. Ao, D., Song, R., Gao, J.: Movement performance of human-robot cooperation control based on EMG-driven hill-type and proportional models for an ankle power-assist exoskeleton robot. *IEEE Trans. Neural Syst. Rehabilitation Eng.* **25**, 8 (2017)
 27. Zhuang, Y., Leng, Y., Zhou, J., Song, R., Li, L., Su, S.W.: Voluntary control of an ankle joint exoskeleton by able-bodied individuals and stroke survivors using EMG-based admittance control scheme. *IEEE Trans. Biomed. Eng.* **68**, 2 (2021)
 28. Liu, H., Tao, J., Lyu, P., Tian, F.: Human-robot cooperative control based on sEMG for the upper limb exoskeleton robot. *Robotics and Autonomous Systems* **125**(2020), 103350 (2020)
 29. Li, Z., Huang, Z., He, W., Su, C.-Y.: Adaptive impedance control for an upper limb robotic exoskeleton using biological signals. *IEEE Trans. Ind. Electron.* **64**(2), 1664–1674 (2017)
 30. Wang, W., Shi, W., Hou, Z.-G., Chen, B., Liang, X., Ren, S., Wang, J., Peng, L.: Prediction of human voluntary torques based on collaborative neuromusculoskeletal modeling and adaptive learning. *IEEE Transactions on Industrial Electronics* **68**, 6 (2021)
 31. Kingma, D.P., Ba, J.L.: Adam: A method for stochastic optimization, International Conference on Learning Representations (ICLR), May 7-9, San Diego, CA, USA (2015)
 32. Lloyd, D.G., Besier, T.F.: An EMG-driven musculoskeletal model to estimate muscle forces and knee joint moments in Vivo. *J. Biomech.* **36**(2003), 765–776 (2003)
 33. Romero, F., Alonso, F.J.: A comparison among different hill-type contraction dynamics formulations for muscle force estimation. *Mechanical Sciences* **7**, 19–29 (2016)
 34. Buchanan1, T.S., Lloyd, D.G., Manal, K., Besier, T.F.: Neuro-musculoskeletal modeling: estimation of muscle forces and joint moments and movements from measurements of neural command. *J. Appl. Biomech.* **20**(4), 367–395 (2004)
- Publisher's Note** Springer Nature remains neutral with regard to jurisdictional claims in published maps and institutional affiliations.
- Pengchen Lian** received his bachelor's degree from University of Science and Technology of China in 2015. He is studying in the Shenzhen Institute of Advanced Technology, Chinese Academy of Sciences for a master's degree at present. His current research interests include artificial intelligence and exoskeleton robot.
- Yue Ma** received his bachelor's and master's degree from Chongqing University of Posts and Telecommunications in 2011 and 2014. He received the Ph. D with the Center for Intelligent and Biomimetic Systems at Shenzhen Institute of Advanced Technology, Chinese Academy of Sciences in 2020. He is working in the Shenzhen Institute of Advanced Technology, Chinese Academy of Sciences as a postdoctoral research fellow at present. His current research interests include artificial intelligence and exoskeleton robot.
- Liangsheng Zheng** received his bachelor's degree from Jiangxi University of Science and Technology in 2015. He is studying in the Shenzhen Institute of Advanced Technology, Chinese Academy of Sciences for a master's degree at present. His current research interests include EEG signal processing and exoskeleton robot.
- Yang Xiao** received his bachelor's degree from Shenyang Ligong University in 2015. He is studying in Chongqing University of Posts and Telecommunications for a master's degree at present. His current research interests include artificial intelligence and exoskeleton robot.
- Xinyu Wu** is now a professor at Shenzhen Institutes of Advanced Technology, and director of Center for Intelligent Bionic. He received his B.E. and M.E. degrees from the Department of Automation, University of Science and Technology of China in 2001 and 2004, respectively. His Ph.D. degree was awarded at the Chinese University of Hong Kong in 2008. He has published over 180 papers and two monographs. His research interests include computer vision, robotics, and intelligent system.

Affiliations

Pengchen Lian^{1,2,3} · Yue Ma^{1,2}  · Liangsheng Zheng^{1,2,3} · Yang Xiao^{1,2,4} · Xinyu Wu^{1,2}

Pengchen Lian
pc.lian@siat.ac.cn

Liangsheng Zheng
ls.zheng@siat.ac.cn

Yang Xiao
xiaoyang@siat.ac.cn

Xinyu Wu
xy.wu@siat.ac.cn

- ¹ Guangdong Provincial Key Lab of Robotics and Intelligent System, Shenzhen Institute of Advanced Technology, Chinese Academy of Sciences, Shenzhen, 518055, Guangdong, China
- ² Guangdong-Hong Kong-Macao Joint Laboratory of Human-Machine Intelligence-Synergy Systems (#2019B121205007), Shenzhen Institute of Advanced Technology, Chinese Academy of Sciences, Shenzhen, China
- ³ University of Chinese Academy of Sciences, Beijing, 100049, China
- ⁴ Chongqing University of Posts and Telecommunications, Chongqing, 400065, China